Journal of Materials Chemistry A

ROYAL SOCIETY OF CHEMISTRY

PAPER

View Article Online
View Journal | View Issue

Cite this: J. Mater. Chem. A, 2025, 13, 25498

Strategies for back contact engineering in high-performance flexible kesterite solar cells†

Carla Gobbo, *[ab] Yuancai Gong, *[cd] Alex Jimenez-Arguijo, [cd] Giorgio Tseberlidis, [a] Vanira Trifiletti, [a] Claudia Malerba, [e] Matteo Valentini, [e] Pau Estarlich, [c] Elaine Armelin, [df] Sonia Lanzalaco, [df] Riccardo Po, [b] Simona Binetti [a] and Edgardo Saucedo [cd]

Kesterite solar cells are pivotal in advancing flexible photovoltaic devices integrated into buildings and products. High-purity Mo foil is one of the most promising flexible substrates, thanks to its outstanding properties. However, the kesterite/Mo foil interface is extremely reactive and chemically unstable during the high-temperature selenization process required to obtain the kesterite crystalline phase, forming a thick $MoSe_2$ layer. The role of $MoSe_2$ in kesterite solar cells is still under discussion, as it can affect the charge extraction at the back contact and the kesterite grain growth. This work reports on the functionalisation of Mo foil to fabricate flexible kesterite solar cells based on Li-doped and Ag-alloyed $Cu_2ZnSn(S,Se)_4$ (Li-ACZTSSe) films grown using the molecular ink method. MoS_2, Al_2O_3, MoO_2, and MoO_3 were inserted between the precursor layer and the substrate to investigate their impact on the $MoSe_2$ thickness, the morphology and composition of the absorber, interface chemistry, carrier collection at the back contact, and the related photovoltaic parameters. It is demonstrated that MoO_3 as an interlayer significant enhances device performance by improving the absorber quality and back contact, achieving an efficiency of 11.2% with a 15 μm thick $MoSe_2$ layer. To the best of our knowledge, this is the first report demonstrating that an over-thick $MoSe_2$ layer is not significantly detrimental to the performance of flexible kesterite-based devices when the Li-ACZTSSe crystallinity and grain growth are improved and its decomposition at the back is prevented.

Received 26th April 2025
Accepted 26th June 2025

DOI: 10.1039/d5ta03303a

rsc.li/materials-a

Introduction

The increasingly urgent need to adopt sustainable alternatives has encouraged the search for solutions to power systems in various application scenarios with solar energy as a renewable source. As a result, flexible thin film photovoltaic (PV) technologies show great potential in different fields, such as building-integrated PV, vehicle-integrated PV, product-integrated PV, indoor applications, and wearable devices, in which the traditional rigid substrate-based solar cells cannot be used due to their high weight and inability to adapt to curved surfaces.[1–5] Among emerging inorganic materials, kesterite $Cu_2ZnSn(S,Se)_4$ (CZTSSe) stands out thanks to its advantageous properties, such as a high absorption coefficient ($>10^4$ cm^{-1}) that enables flexible light absorber thin films (~1–2 μm), low-cost and environmentally friendly constituents, direct and tunable bandgaps (E_g = 1.0–1.5 eV, depending on the [S]/([S] + [Se]) ratio), and long-term stability. Moreover, Se-rich CZTSSe films with a bandgap of around 1.1 eV offer promising opportunities to be employed as a bottom cell in a flexible tandem device to maximize the efficiency (η) and make it more suitable for industrial level and commercial applications.[6–8]

Several flexible substrates, including metals (*e.g.*, Mo, stainless steel, Ni, Cu, Ti, and Al), plastics (*e.g.*, polyimide), and ceramics (*e.g.*, flexible glass and ZrO_2), have been studied and reported for CZTSSe-based devices.[3,5] Compared to the others, high-purity Mo foil excels due to its high-temperature resistance, good mechanical strength, high conductivity, and lack of metallic impurities.[9] Furthermore, CZTSSe thin films grown on Mo foil exhibit enhanced crystallinity.[3,10] Moreover, the Mo foil

[a]Department of Materials Science and Solar Energy Research Center (MIB-SOLAR), University of Milano-Bicocca, Via Roberto Cozzi 55, 20125 Milan, Italy. E-mail: c.gobbo3@campus.unimib.it

[b]Eni S.p.A - New Energies, Renewable Energies and Materials Science Research Center, 28100 Novara, Italy

[c]Photovoltaic Group, Electronic Engineering Department, Polytechnic University of Catalonia (UPC), Av. Eduard Maristany, 16, 08019 Barcelona, Spain. E-mail: yuancai.gong@upc.edu

[d]Universitat Politècnica de Catalunya (UPC), Barcelona Centre for Multiscale Science & Engineering, Av Eduard Maristany 10-14, Barcelona, 08019, Spain

[e]ENEA (Agenzia Nazionale per le Nuove Tecnologie, l'Energia e lo Sviluppo Economico Sostenibile) C.R. CASACCIA, Via Anguillarese 301, 00123 Rome, Italy

[f]IMEM-BRT's Group, Departament d'Enginyeria Química, EEBE, Universitat Politècnica de Catalunya, C/Eduard Maristany, 10-14, Ed. I, 2nd Floor, 08019 Barcelona, Spain

† Electronic supplementary information (ESI) available. See DOI: https://doi.org/10.1039/d5ta03303a

can act both as a substrate and a back contact.[5] Regardless of the substrate type, achieving high efficiencies in CZTSSe solar cells is a significant challenge due to the formation of defects and secondary phases in the absorber,[11] and severe recombination at the kesterite/buffer interface,[12–14] leading to a large open-circuit voltage (V_{OC}) deficit and efficiency loss. Recently, record efficiencies of 15.8% on conventional rigid soda-lime glass (SLG)[15] and 12.8% on flexible Mo foil[16] have been achieved using a molecular ink-based absorber synthesis approach. Although the efficiency gap between flexible and rigid kesterite-based solar cells is closing rapidly, as discussed in this work, additional requirements are needed when a flexible substrate is used.[1]

One of the main challenges with flexible Mo foil is the lack of alkali metal elements in the substrate (present instead in SLG), typically needed to promote kesterite crystallisation, adjust carrier concentration, passivate grain boundaries, and enhance adhesion to the foil.[1,17,18] Alkali element doping[6,17] (*e.g.*, Na, Li, and K), combined with substitutional alloying (*e.g.*, Ag),[19] plays a key role in facilitating grain growth, enhancing absorber crystallinity, and regulating detrimental defects to achieve high-efficiency flexible kesterite-based devices.[20] Little research has focused on the combined effect of Li doping and Ag substitution, with most studies centred on SLG-based devices.[20]

Another crucial factor influencing flexible solar cell performance is the absorber/Mo foil interface, which impacts electronic properties, kesterite morphology, and secondary phase formation. The role of the interplay between formation, thickness, and doping of $MoSe_2$ in flexible Mo foil-based CZTSSe solar cells remains unclear. During the high-temperature thermal process under a large excess of selenium, required to obtain the crystalline CZTSSe phase, forming a thick $MoSe_2$ layer is inevitable.[21] As shown in this work, when the Mo foil is used both as a substrate and as a back contact, the formation of the $MoSe_2$ interface layer is even more favoured due to the substrate's crystal-preferred orientation and high reactivity.[22] The $MoSe_2$ growth can follow two different reaction pathways, as reported below:

$$Mo + Se_2(g) \rightarrow MoSe_2 \quad (1)$$

$$2Cu_2ZnSnSe_4 + Mo \rightarrow 2Cu_2Se + 2ZnSe + 2SnSe + MoSe_2 \quad (2)$$

The free energy change determined at 550 °C for reactions (1) and (2) is −186 kJ mol^{-1} and −100 kJ mol^{-1}, respectively, indicating that the CZTSSe/Mo interface is reactive and unstable under such conditions.[21,23] Typically, a thin $MoSe_2$ layer forms a good ohmic contact, while an over-thick one increases the carrier recombination at the rear interface and reduces the hole transport. However, this might be related to its conductivity, as $MoSe_2$ shows both p-type and n-type electrical properties depending on different possible dopants incorporated into the film (*e.g.*, O, Zn, P, Nb, Va, and Ta give p-type doping, while Re and Cs induce n-type doping).[24,25] In the first case, the back contact properties of the CZTSSe device are improved, and the electronic structure of $MoSe_2$ is optimised. At the same time, hole transfer is prevented in the latter, and the carrier recombination is enhanced. A variety of back contact diffusion barriers, including metal oxides, sulfides and nitrides, have been investigated to prevent Se diffusion to the back contact in CIGS and CZTS solar cells.[26,27] To improve the back contact, many blocking and sacrificial layers, typically with a high work function, such as Al_2O_3, TiN, TiB_2, MoO_x, Ag, Bi, MoS_2, ZnO, WO_3, a-SiC, and CuO, have been deposited between CZTSSe/CIGS and Mo.[23,24,28–32] However, although $MoSe_2$ formation and back contact engineering are more critical in Mo foil-based kesterite solar cells, most previous studies have focused on regulating the kesterite/$MoSe_2$/Mo interface on rigid SLG substrates.[33–35]

In general, previous studies have devoted extensive efforts to improving flexible kesterite solar cells through (1) alkali doping to enhance absorber crystallization and defect passivation on alkali-free Mo foil;[36] (2) surface treatments of Mo foil—such as electrochemical polishing, plasma,[37] or ozone exposure,[38]—to reduce roughness and improve substrate wettability; and (3) interface engineering of the kesterite/CdS heterojunction to suppress interfacial recombination.[16,39] However, regulation of the back interface in flexible kesterite solar cells remains underexplored. While several reports have demonstrated that inserting barrier or sacrificial layers at the absorber/Mo interface improves performance on rigid SLG substrates, these strategies are not directly transferrable to flexible devices due to the distinct crystallographic texture, reactivity, and thermal expansion behavior of Mo foil compared to Mo coated on glass.

To address these critical issues, this work presents the first systematic study that combines alkali (Li) doping and back contact engineering—through the introduction of four different interlayers (MoS_2, MoO_2, MoO_3, and Al_2O_3)—to enhance the performance of flexible CZTSSe solar cells. The study systematically investigates these interfacial layers, examining their influence on $MoSe_2$ thickness and growth mechanisms (reaction (1) or (2)) on flexible Mo foil, their effect on carrier transportation at the back contact, their impact on Li-ACZTSSe crystallization and film quality, and their ability to suppress kesterite decomposition at the back interface (reaction (2)). As a result, a flexible kesterite solar cell with 11.2% efficiency was achieved by fabricating a Li-doped kesterite absorber on Mo foil coated with a MoO_3 layer. Compared to other interlayers, MoO_3 significantly improves film uniformity by enhancing the solution's wettability on the foil, suppresses reaction (2), and promotes uniform and compact grain growth, leading to a higher V_{OC} and fill factor (FF). More importantly, to the best of our knowledge, this is the first report demonstrating that a 15 μm $MoSe_2$ layer is not detrimental to device performance when absorber and back contact quality are sufficiently improved through effective back contact engineering.

Results and discussion

The absorber optimisation by introducing Li, with a nominal Li/(Cu + Ag) ratio of 0.02, is provided and discussed in the ESI.† The methodology followed was previously studied for devices on rigid SLG substrates.[20,40,41] Li dopant has been reported to preferentially occupy Zn/Cu sites, forming Li_{Zn} antisite defects

or V_{Cu}, which can increase hole concentration and enhance p-type conductivity.[42] Moreover, Li at grain boundaries can reduce defect density and passivate recombination centers, thereby improving carrier collection and reducing recombination.[43] These effects are particularly beneficial in flexible CZTSSe devices, where alkali elements such as Na are typically absent.[44] The Li-doping level was confirmed by GDOES measurement (Fig. S1a, ESI†). As depicted in Fig. S1b and c (ESI†), the absorbers show good crystalline quality and no secondary phases. Additionally, the Li dopant promoted the coalescence of the kesterite grains, thus enhancing adhesion to the flexible substrate, increasing shunt resistance (R_{Sh}), and improving charge extraction at the back contact (Fig. S1d and e in the ESI†). The *J*–*V* and EQE results presented in the ESI (Fig. S2a–g and Table S1†) confirm that Li-doping can greatly improve the PV performance of flexible ACZTSSe devices, leading to up to 10.4% efficiencies. As shown in Fig. 1a and b, the so-produced devices present a thick $MoSe_2$ layer (over 15 μm) on flexible Mo foil, compared to the one on the rigid SLG substrate, with a thickness of 800 nm. Moreover, it can be noted that the $MoSe_2$ thickness is not uniform and constant when the flexible substrate is employed. According to Lin *et al.*,[22] the crystallographic orientation of the Mo substrate highly influences its reactivity with the Se atmosphere (reaction (1)). It affects the chemical stability of the ACZTSSe/Mo interface, ultimately leading to kesterite decomposition (reaction (2)). Fig. 1c confirms that the flexible Mo foil has dominant (200) and (211) plane orientations at $2\theta = 58.6$ deg and $2\theta = 73.7$ deg, respectively, with a lower planar packing factor and more Mo atoms exposed and ready to react with Li-ACZTSSe or the Se atmosphere during the annealing process.[22]

In contrast, the sputtered Mo layer, typically deposited as the back contact when SLG is used as substrate, has a (110) preferred orientation at $2\theta = 40.6$ deg, implying reduced Se reactivity with the Mo layer and limited $MoSe_2$ formation. Therefore, the functionalisation of the Mo foil with MoS_2, Al_2O_3, MoO_3, and MoO_2 as interfacial layers between the flexible substrate and the absorber was tested to prevent the potentially detrimental reactions (1) and (2), as schematized in Fig. 1d. Phase identification of the introduced interlayers was performed by XRD and Raman spectroscopy, as shown in Fig. S3a–c (ESI†). The Raman spectra of the Li-ACZTSSe synthesised on all the different functionalised flexible substrates are presented in Fig. 2a. Regardless of the interlayer employed, typical kesterite Raman peaks are detected,[45] confirming good Li-ACZTSSe quality without evident secondary phases. XRD measurements

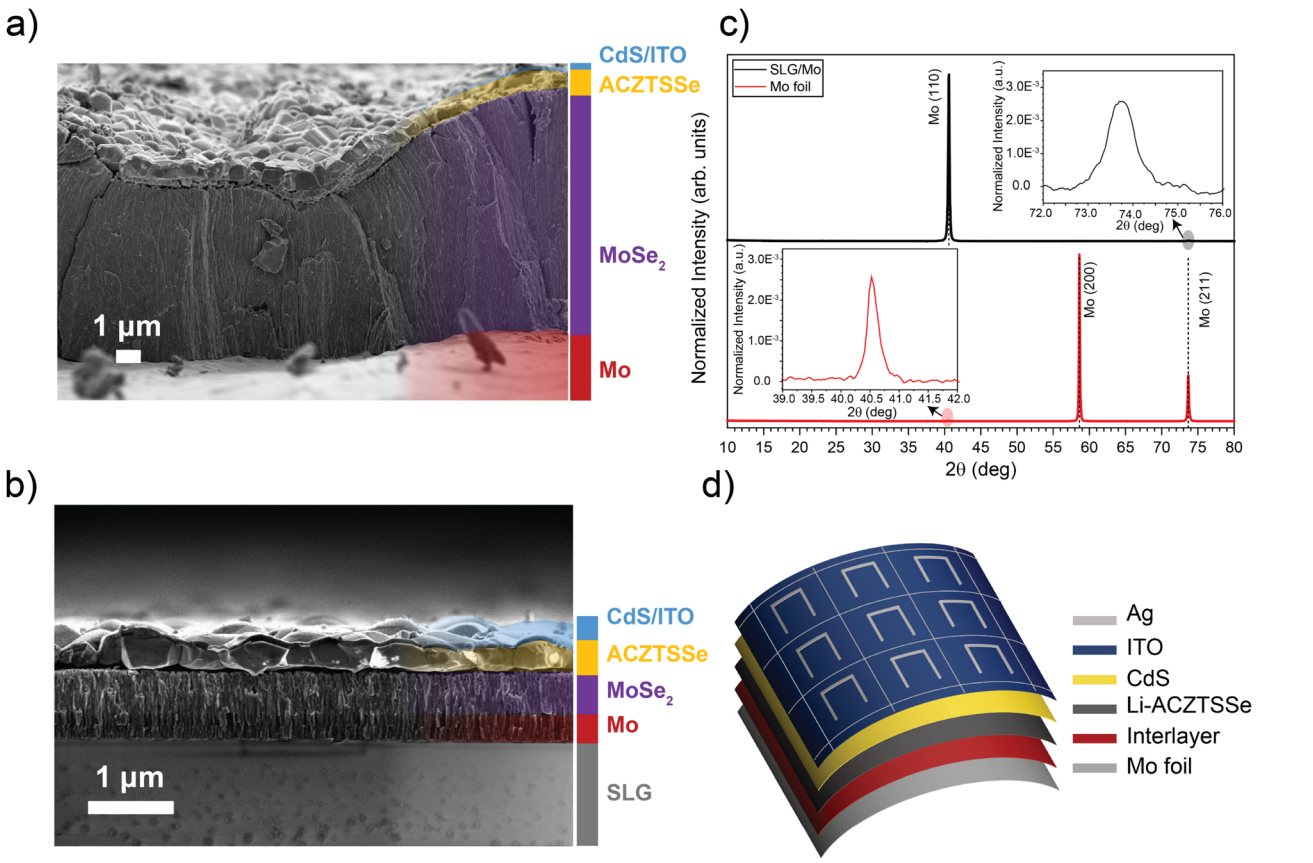

Fig. 1 Cross-sectional Scanning Electron Microscopy (SEM) images of kesterite-based devices grown on (a) flexible Mo foil and (b) SLG/Mo rigid substrates. Starting from the bottom to the top, the layers are highlighted as follows: SLG in grey, Mo in red, $MoSe_2$ in purple, Li-ACZTSSe in yellow, and CdS and TCO in blue. (c) Comparison between the XRD patterns of the SLG/Mo rigid substrate (in black) and flexible Mo foil (in red): the Mo layer sputtered on SLG has (110) preferred orientation, while the flexible Mo foil has dominant (200) and (211) orientations. (d) Schematic representation of the Li-ACZTSSe device architecture based on flexible functionalised Mo foil.

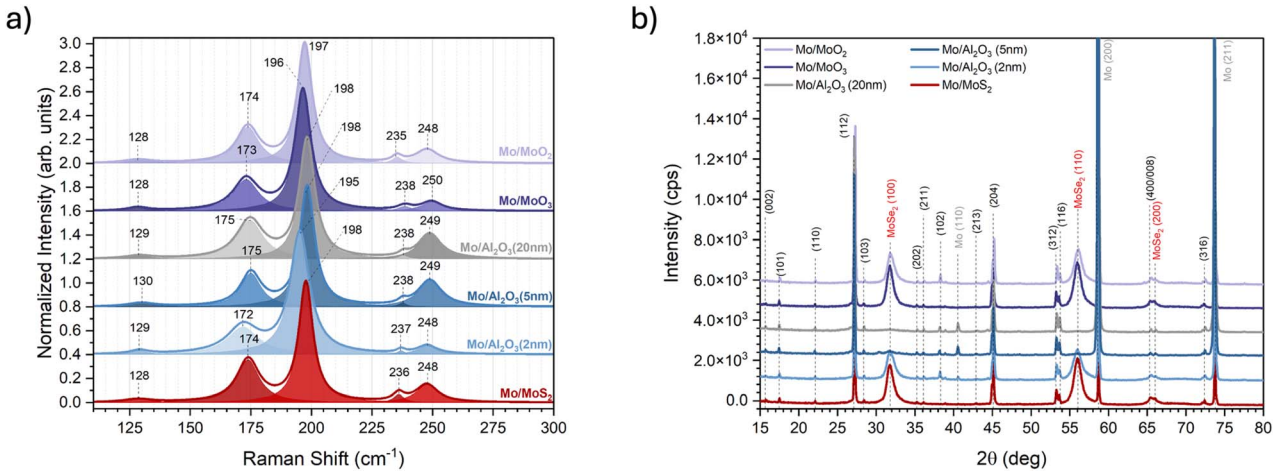

Fig. 2 (a) Deconvoluted Raman peaks and (b) crystallographic patterns of Li-ACZTSSe-based devices on flexible Mo foil with MoS_2 (dark red line), 2 nm Al_2O_3 (light blue line), 5 nm Al_2O_3 (blue line), 20 nm Al_2O_3 (grey line), MoO_3 (purple line), and MoO_2 (lilac line) as interfacial layers.

were then performed as complementary analyses to Raman spectroscopy. The XRD patterns of the Li-ACZTSSe samples on the flexible substrates are presented in Fig. 2b. Good Li-ACZTSSe crystalline quality is confirmed by the presence of sharp peaks related to the kesterite phase, regardless of the interlayer used. Furthermore, it is possible to evaluate through XRD how the different interlayers affect the thickness of $MoSe_2$ on the substrate by assessing the intensity of the (100), (110), and (200) peaks of $MoSe_2$ at $2\theta = 31.8$ deg, $2\theta = 56.0$ deg, and $2\theta = 66.1$ deg, respectively. When MoS_2 is intentionally grown on the flexible foil, due to its preferred orientation perpendicular to the plane of the substrate, Se vapour readily diffuses through the S–Mo–S planes to the Mo foil, thus forming a thick $MoSe_2$ layer.[46] Reducing the Se diffusion wholly or partially to the flexible substrate can be achieved by introducing Al_2O_3 with different thicknesses. The thickest Al_2O_3 interlayer (20 nm) effectively prevents the formation of $MoSe_2$, and the one with intermediate thickness (5 nm) shows weak $MoSe_2$ signals. In comparison the thinnest layer (2 nm) allows $MoSe_2$ growth, but with lower-intensity peaks compared to the other interlayers. In the last case, mechanical defects like cracks in the interlayer might limit diffusion barrier properties due to the deposition of ultrathin Al_2O_3 on a moderately rough Mo foil surface.[24] Interestingly, although it is reported in the literature that MoO_x can suppress Se diffusion toward Mo,[47,48] both MoO_2 and MoO_3 do not exhibit blocking layer behaviour and have no effect on reducing the $MoSe_2$ thickness.

The $MoSe_2$ thickness was also determined using GDOES analysis (see Fig. S4a–e, ESI†). Consistent with the XRD pattern, the samples with an Al_2O_3 interlayer show a thinner $MoSe_2$ layer, followed by the reference sample produced directly on Mo foil. The sample with the MoS_2 interlayer exhibits an almost double $MoSe_2$ thickness compared to the reference. On the other hand, the devices with MoO_3 and MoO_2 interlayers display very similar $MoSe_2$ thicknesses, close to that obtained on bare Mo foil. GDOES measurements also assessed elemental distributions across the device stack (Fig. 3a–e). The Cu, Ag, Zn, Sn, and Se profiles within the absorber appear consistent across all samples, suggesting that variations in the interlayer composition have limited influence on bulk elemental uniformity. In the interphase region between Li-ACZTSSe and $MoSe_2$, signals corresponding to kesterite-related cations are detected in all cases. Notably, samples incorporating bare Mo foil or MoO_2 exhibit more pronounced diffusion of the kesterite elements into the back contact (Fig. 3a and e), which is consistent with interfacial reactions that may lead to kesterite decomposition (reaction (2)) and the formation of secondary phases such as ZnSe, SnSe, $Mo(S,Se)_2$, *etc.* Besides, Cu and Se diffusion toward the back contact can impact the absorber/back contact interface, forming Sn- and Zn-related defects and V_{OC} losses. In contrast, interlayers such as MoS_2, MoO_3, and Al_2O_3 have been reported to act as effective diffusion barriers, helping to limit these interfacial reactions and improve absorber stability.[32,49,50]

These trends are reflected in the GDOES profiles shown in Fig. 3a and d, suggesting sharper interfacial gradients and reduced diffusion of kesterite metal cations at the back interface in samples containing diffusion-limiting interlayers. The interlayers not only play a key role in the $MoSe_2$ thickness and the Li-ACZTSSe/Mo interfacial region but can also affect the absorber nucleation and growth. As shown in Fig. 4a–e, the grain size of Li-ACZTSSe depends on the interlayer used. Compared to the reference on bare Mo foil, almost no effect is observed when MoS_2 and MoO_2 are used, suggesting that they induce similar kesterite nucleation and grain growth processes. In contrast, Al_2O_3 leads to reduced grain size, while MoO_3 enhances it. To understand this, wetting contact angle (WCA) measurements were performed, showing that grain growth might be related to the wettability,[51] and therefore the surface energy, of the functionalised Mo foil substrates. As shown in the ESI (Fig. S5a–e†), MoS_2 and MoO_2 exhibit wettability comparable to the bare Mo foil, leading to similar absorber morphology and $MoSe_2$ growth. The lower wettability of the Al_2O_3 layer might hinder the absorber grain growth during selenization, resulting in non-uniform crystallization. In

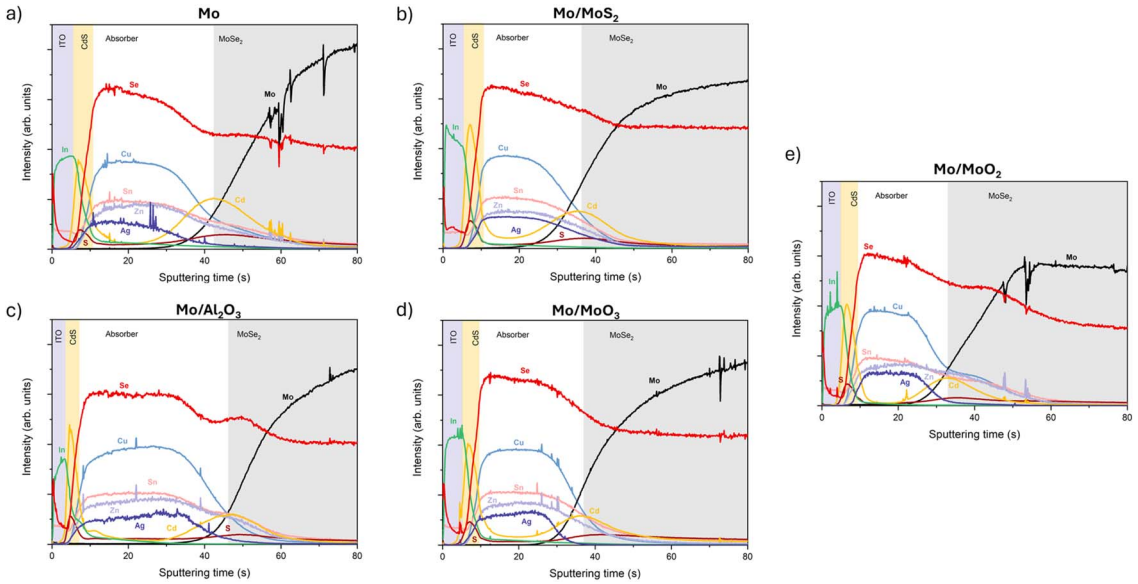

Fig. 3 GDOES profiles of devices with (a) Mo foil, (b) Mo foil/MoS_2, (c) Mo foil/2 nm Al_2O_3, (d) Mo foil/MoO_3, and (e) Mo foil/MoO_2 as substrates.

contrast, the improved Li-ACZTSSe grain size detected when MoO_3 is inserted can be related to its enhanced wettability, which might aid grain growth and promote kesterite adhesion to the foil. Moreover, its lower WCA seems to induce a more continuous and uniform bottom precursor layer, with reduced lattice strain, which can facilitate the growth of larger coherent grains in the final bottom absorber layer (Fig. 1a).

Another beneficial effect on the Li-ACZTSSe crystalline quality introduced by MoO_3 could be the role of oxygen in defect passivation, as during the high-temperature selenization process, it can be supplied from the interlayer and fill chalcogen vacancies.[52] Finally, the impact of the different interlayers on majority carrier collection at the back contact and on the final PV performance was studied. Devices with 5 and 20 nm Al_2O_3 resulted in non-working solar cells due to the introduction of a thicker resistive interlayer. The statistical photovoltaic parameters of devices fabricated without an interlayer (reference) and those incorporating various interlayers are presented in Fig. 5a–d. Fig. 5e and f displays representative *J–V* curves of the devices, and their PV parameters are summarised in Table 1. When MoS_2 is intentionally deposited on the Mo foil, in agreement with the formation of an over-thick $MoSe_2$ layer confirmed by XRD and GDOES results, there is a drop in all the PV parameters ($\eta = 7.8\%$) due to the severe deterioration of the back contact. The devices with a 2 nm Al_2O_3 barrier exhibit a significant improvement in short-circuit current density (J_{SC}),

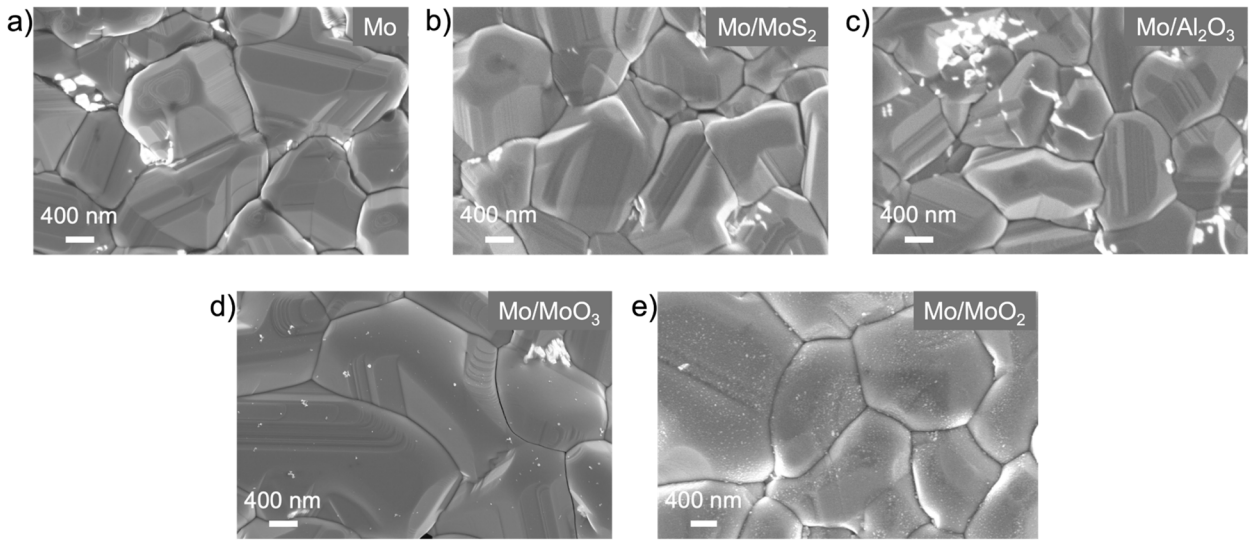

Fig. 4 Top-view SEM images of the absorbers grown on (a) Mo foil, (b) Mo foil/MoS_2, (c) Mo foil/2 nm Al_2O_3, (d) Mo foil/MoO_3, and (e) Mo foil/MoO_2.

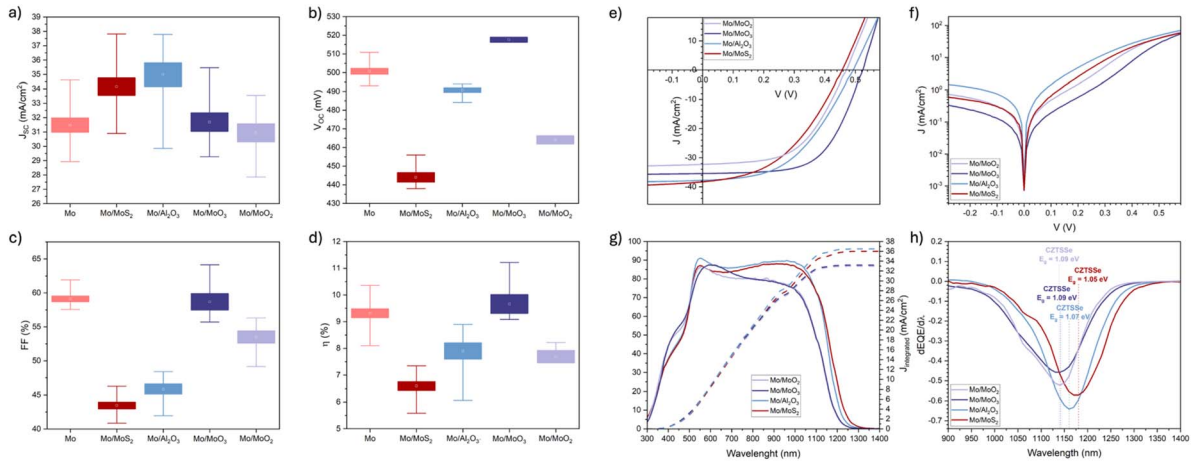

Fig. 5 Box plot of (a) J_{SC}, (b) V_{OC}, (c) FF, (d) η for devices produced on Mo bare foil (in pink), Mo foil/MoS_2 (in dark red), Mo foil/2 nm Al_2O_3 (in light blue), Mo foil/MoO_3 (in purple), and Mo foil/MoO_2 (in lilac). (e) Illuminated and (f) dark J–V curves, (g) EQE measurements, and (h) estimated electronic bandgap of the champion Li-ACZTSSe-based devices with MoS_2 (in dark red), 2 nm Al_2O_3 (in light blue), MoO_3 (in purple), and MoO_2 (in lilac) as interlayers.

attributed mainly to reduced elements diffusion from the absorber to the Mo foil and, consequently, enhanced kesterite quality near the back interface.

However, due to the insulating properties of Al_2O_3, resistive losses increase, resulting in a reduced fill factor (FF) and limiting the device efficiency to 8.9%. Indeed, according to previous studies,[50,53] this dense and dielectric Al_2O_3 interlayer effectively blocks Se diffusion and prevents the contact between the absorber and Mo foil. This significantly suppresses $MoSe_2$ formation (reaction (1)) and inhibits kesterite decomposition (reaction (2)) during high-temperature selenization, ensuring the formation of a thin and controlled $MoSe_2$ layer. However, it hinders the direct connection between the absorber and $MoSe_2$, which is essential for the ohmic hole contact. To improve the ohmicity at the back contact, nano-openings/patterns could be created in the Al_2O_3 passivation layer.[50] Moreover, the lower wettability of the substrate, which limits absorber grain growth, contributes to a reduced V_{OC}.

In contrast, MoO_3 insertion has a beneficial effect on both the FF and the V_{OC}. However, the improvement in PV performance ($\eta = 11.2\%$) cannot be attributed to the ability of this interlayer to inhibit $MoSe_2$ formation but rather to its role in better promoting a controlled Li-ACZTSSe film composition and grain growth, which are strongly related to the $MoSe_2$ formation dynamics. This suggests $MoSe_2$ growth mainly through reaction (1), thereby preventing absorber decomposition. Despite its extension, $MoSe_2$ acts as a good hole transport layer (HTL), suggesting that, when MoO_3 is used as a sacrificial layer, O-doping from the initial oxide layer might enhance the electrical properties and the p-type behaviour of the resulting $MoSe_2$.[54] Indeed, it has been demonstrated in the literature that the passivation of S and Se vacancies by oxygen can enhance the p-type doping of $Mo(S,Se)_2$.[52,55] Furthermore, the MoO_3 layer can modify the band alignment at the back contact, leading to improved majority carrier extraction.[56] Additionally, the V_{OC} enhancement can be ascribed to the higher wettability of the substrate and, therefore, to the improved Li-ACZTSSe grain growth.

In contrast, when MoO_2 is employed, severe decomposition of the absorber at the back contact and significant diffusion of kesterite metal cations into the $MoSe_2$ layer result in lower PV parameters ($\eta = 8.2\%$), suggesting that the Mo–O phase and fine-tuning the oxygen content in the initial oxide interlayer is crucial for achieving good p-type $MoSe_2$ and promoting kesterite crystallisation and grain growth. A single-diode model analysis was also performed (Table 1). Devices with the MoO_3 interlayer exhibited a low diode ideality factor ($n = 1.86$) and the lowest saturation current density ($J_0 = 6.2 \times 10^{-7}$), indicating reduced recombination and superior absorber quality. In contrast, MoS_2 and MoO_2 interlayers resulted in higher n (>2) and J_0, suggesting increased recombination respectively due to significant substrate or absorber decomposition at the back

Table 1 J–V parameters and diode analysis for representative Li-ACZTSSe solar cells incorporating different interfacial layers between the absorber and flexible Mo foil

Interlayer	J_{SC} (mA cm^{-2})	$J_{integrated}$ (mA cm^{-2})	V_{OC} (mV)	FF (%)	η (%)	R_S (Ω cm^2)	R_{Sh} (Ω cm^2)	J_0 (A cm^{-2})	n
Reference	34.6	33.9	510	58.6	10.4	1.6	538	1.77×10^{-6}	2.01
MoS_2	38.3	36.0	457	44.3	7.8	2.98	436	1.64×10^{-5}	2.31
Al_2O_3	37.8	36.5	493	47.7	8.9	3.28	245	5.70×10^{-6}	2.13
MoO_3	35.5	33.3	528	59.9	11.2	1.57	632	6.20×10^{-7}	1.86
MoO_2	32.3	33.0	466	54.5	8.2	2.61	265	1.04×10^{-6}	1.77

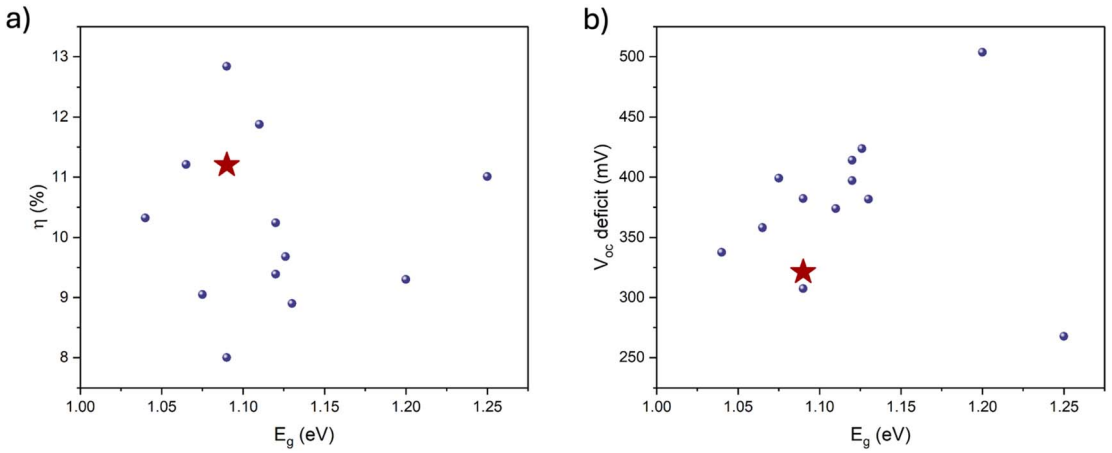

Fig. 6 (a) Record efficiencies of kesterite solar cells on flexible Mo foil and (b) V_{OC} deficit of the corresponding devices as a function of E_g.[16–18,39] The results of this work are highlighted with a red star.

contact and non-optimal grain growth during the selenization process. As discussed earlier, the dielectric Al_2O_3 interlayer yielded intermediate diode parameters and device performance, effectively minimising interface decomposition, elemental diffusion from the absorber to the Mo back contact, and $MoSe_2$ thickness, but introducing significantly higher series resistance (R_S). The lowest R_S was determined for the MoO_3-based devices, thus contributing to improved hole transport and enhanced FF (~60%). In contrast, MoS_2 and MoO_2 interlayers considerably raised R_S, while the Al_2O_3 barrier further increased it due to its dielectric nature. Furthermore, the MoO_3 sacrificial layer provided the highest shunt resistance (R_{Sh}), confirming minimised leakage currents due to improved absorber uniformity and quality. Overall, the MoO_3 interlayer optimised back contact properties, reduced recombination, and promoted beneficial grain growth.

These results highlight the critical role of controlled back contact engineering in enhancing flexible kesterite solar cell performance. The changes in the current collection are assessed by EQE and are reported in Fig. 5g. The EQE spectra can be divided into two distinct regions: the buffer and window layer absorption effect zone (300–520 nm) and the exclusive Li-ACZTSSe absorption region (520–1200 nm). All devices exhibit similar spectral responses within the 300–520 nm range, indicating consistent properties of the buffer and window layers across the devices. Similar spectra are obtained when MoO_2 and MoO_3 are employed, suggesting a comparable band structure. Devices with Al_2O_3 and MoS_2 interlayers show higher carrier collection in the 550–1200 nm range. This enhancement likely arises from a reduction in defects within the absorber and improved interface quality at the Li-ACZTSSe/buffer junction, consistent with the decreased elemental diffusion observed at the back contact. Consequently, a longer electron diffusion length and more efficient minority carrier collection are achieved. Moreover, Al_2O_3, already well known in the literature as a rear passivation intermediate layer,[53] can successfully inhibit the detrimental interfacial reaction between kesterite and flexible Mo foil, thereby preventing the related electron losses. Interestingly, the lower EQE values for both MoO_2 and MoO_3 layers indicate higher collection losses at the back interface. Therefore, the improved efficiency with MoO_3 may result from enhanced crystallinity and grain quality, leading to a higher V_{OC} and FF. This highlights the importance of controlling grain growth and back-contact properties *via* an interlayer when fabricating kesterite devices on flexible substrates. Further deposition of a thin, nanopatterned Al_2O_3 layer on Mo foil may offer a promising strategy to suppress excessive $MoSe_2$ formation while maintaining adequate charge transport, thereby improving device performance. Fig. 5h presents the evaluated electronic bandgaps, which, with slight variations, are close to the expected value (1.1 eV) in all cases. In conclusion, the MoO_3 interlayer led to a maximum device performance of 11.2%, among the best devices reported in the literature (Fig. 6a and Table 2).

Furthermore, the voltage deficit (V_{OC}^{def}) of the champion device, evaluated using $V_{OC}^{def} = V_{OC}^{SQ} - V_{OC}^{measured}$, where $V_{OC}^{SQ} =$

Table 2 Summary of efficiencies for flexible kesterite solar cells on various substrates, compared with record devices on SLG

Substrate	Process	Strategies	Absorber	η (%)	Ref.
Mo foil	Molecular ink	MoO_3 interlayer	$(Ag,Cu)_2ZnSn(S,Se)_4$	11.2	This work
Mo foil	Molecular ink	Rb-doped ACZTSSe/CdS	$(Ag,Cu)_2ZnSn(S,Se)_4$	12.84	16
Stainless steel	Sputtering	SiO_2 barrier	$Cu_2ZnSn(S,Se)_4$	10.3	57
Ti foil	Molecular ink	Cd alloying	$Cu_2(Zn,Cd)SnS_4$	6.51	58
Polyimide	Sputtering	Na–Ge co-doping	$Cu_2ZnSnSe_4$	4.9	59
Rigid SLG	Molecular ink	n/a	$(Ag,Cu)_2ZnSn(S,Se)_4$	15.8	15

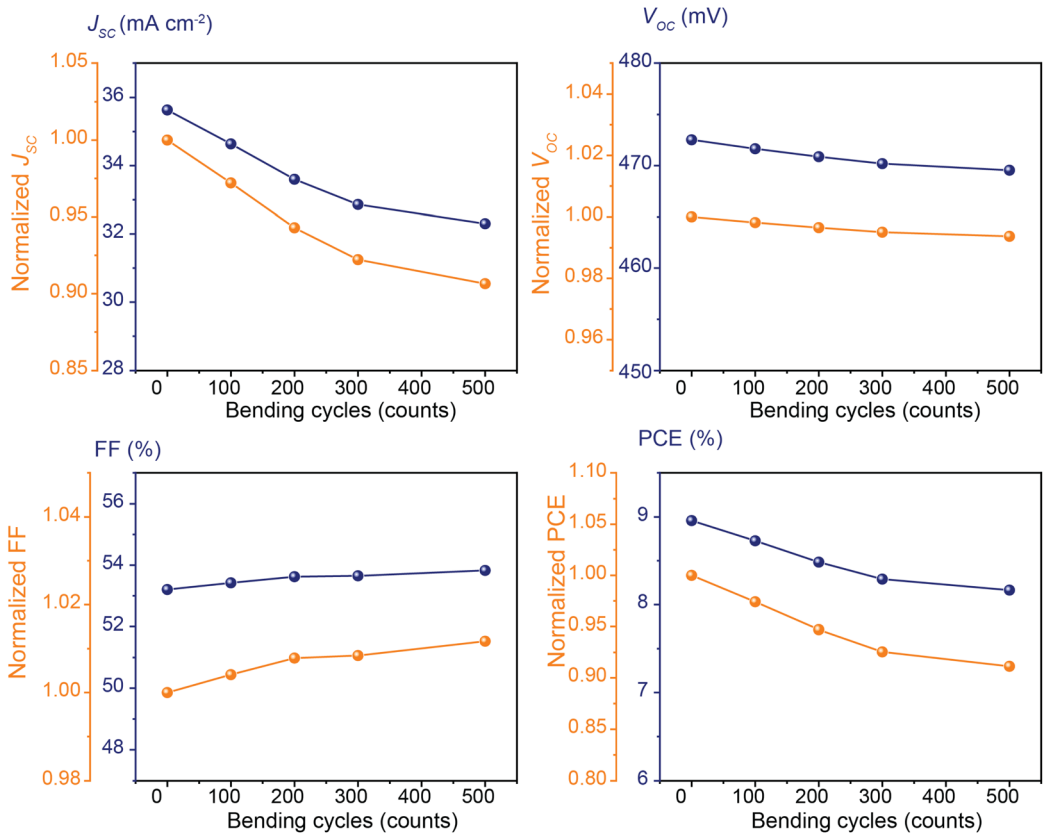

Fig. 7 Photovoltaic parameters of flexible kesterite solar cells fabricated on Mo/MoO_3 substrates after bending tests with varying cycle counts (bending radius fixed at 1 cm for 2.5 × 2.5 cm^2 devices). Changes in J_{SC}, V_{OC}, FF, and PCE are shown, along with their normalized values.

0.932 E_g/q − 0.1667 V,[20] is one of the lowest in the literature, as shown in Fig. 6b. Table 2 summarizes representative high-efficiency kesterite solar cells fabricated on various substrates—including rigid SLG, Mo foil, Ti foil, stainless steel, and polyimide—and compares them with the results of this study. As shown, a significant performance gap remains between rigid (15.8%) and the flexible devices (11.2%). This gap is primarily attributed to $MoSe_2$ overgrowth, stress-induced crystallization issues, and stoichiometric imbalances on flexible substrates. To address these challenges, further improvements may involve nano-patterned Al_2O_3 interlayers, stress-relief buffer layers, alkali co-doping, and passivation of the kesterite/CdS interface. Additionally, as shown in Fig. 7, bending tests were performed on devices with MoO_3 as an interlayer. Under bending conditions with a radius of 1.0 cm for 2.5 × 2.5 cm^2 devices, the flexible solar cells retained over 90% of their initial efficiency after 500 cycles. Both V_{OC} and FF remained highly stable, with less than 1% loss, confirming the excellent mechanical resilience of the kesterite absorber and the engineered back interface. The primary source of efficiency loss was a decrease in J_{SC} (over 8%), which is attributed to the fixed bending curvature during measurement after cycling. This likely reduced the effective light absorption due to changes in the incident angle and light path, rather than degradation of the device itself. The devices maintained stable and durable performance under the bending condition. The high-efficiency flexible devices were stored under ambient conditions without encapsulation. After 90 days, the devices exhibited less than 2% PCE degradation as shown in Fig. S6,† demonstrating good long-term stability.

Conclusions

This study investigated the integration of Li-doped CZTSSe absorbers and various back contact engineering strategies to enhance the performance of flexible kesterite solar cells. Four interlayers (MoS_2, Al_2O_3, MoO_2, and MoO_3) were evaluated at the interface between the Mo foil substrate and the absorber.

The results demonstrate that Li doping significantly improves device efficiency from 8.5% to 10.4%. And each interlayer has a specific impact on the $MoSe_2$ thickness and growth, Li-ACZTSSe crystallisation, grain size and quality, charge extraction at the back contact, and the PV parameters of the device. MoS_2 insertion leads to the formation of an over-thick $MoSe_2$ byproduct and a reduction in all the PV parameters. In contrast, Al_2O_3 is an effective blocking layer, capable of wholly or partially reducing the Se diffusion to the back contact and tuning the $MoSe_2$ thickness. Moreover, Al_2O_3 inhibits the detrimental interfacial reaction between the absorber and the substrate. However, Al_2O_3 introduces resistive losses and limits the absorber grain growth due to its lower wettability, leading to non-optimal crystallisation and a reduced FF and V_{OC}. When

MoO_2 is used, severe kesterite degradation at the rear interface results in lower PV parameters. In contrast, MoO_3 is the most promising interlayer and an effective strategy, achieving an efficiency of 11.2%. The improvement in the final device performance can be ascribed to three main factors. (i) MoO_3 reduces the rear interface decomposition and mitigates reaction (2) more successfully than other interlayers. (ii) The resulting thick $MoSe_2$ layer is tolerable and not detrimental to PV performance, thanks to MoO_3's influence on its growth mechanism, primarily through the direct reaction between Mo and Se (see reaction (1)), and to O-doping. (iii) MoO_3 enhances substrate wettability, thus promoting the formation of larger kesterite grains and improving the FF and V_{OC} more effectively than the other strategies explored. These results highlight the crucial role of back contact engineering in enhancing flexible kesterite solar cell performance. To the best of our knowledge, this is the first report demonstrating that an over-thick (15 μm) $MoSe_2$ layer does not negatively affect the performance of flexible kesterite-based solar cells if the absorber grain size, composition, and quality are optimised. Furthermore, compared to the deposition methods of the other interlayers investigated, pre-annealing the flexible Mo foil in air is easier and more straightforward, and does not require sophisticated or expensive equipment, making this process appealing and suitable for industrial scale-up implementation. In conclusion, the findings reported in this work offer promising prospects for further advancements in flexible kesterite-based devices, paving the way for future optimizations and potential large-scale integrated PV applications.

Data availability

The authors confirm that the data supporting the findings of this study are available within the article or its ESI.†

Author contributions

Carla Gobbo: writing – original draft, writing – review & editing, visualization, validation, methodology, investigation, data curation, conceptualization. Yuancai Gong: writing – original draft, writing – review & editing, resources, methodology, investigation, conceptualization. Alex Jimenez-Arguijo: writing – original draft, writing – review & editing, resources, methodology, investigation, conceptualization. Giorgio Tseberlidis: writing – review & editing, validation, supervision. Vanira Trifiletti: writing – review & editing, validation. Claudia Malerba: investigation, formal analysis. Matteo Valentini: investigation, formal analysis. Pau Estarlich Gil: investigation, formal analysis. Elaine Armelin: investigation, formal analysis. Sonia Lanzalaco: investigation, formal analysis. Riccardo Po: writing – review & editing, supervision, funding acquisition. Simona Binetti: writing – review & editing, supervision, funding acquisition. Edgardo Saucedo: writing – review & editing, supervision, resources, project administration, funding acquisition.

Conflicts of interest

There are no conflicts to declare.

Acknowledgements

This project received funding from the European Union's H2020 ERC-Consolidator programme under grant agreement number no. 866018 (SENSATE), and from the Science and Innovation Ministry of Spain projects PID2023-148976OB-C41 (CURIO-CITY) and PCI2023-145971-2 (ACT-FAST, CET-Partnership 2023 program). C. G. thanks Eni S.p.A. for funding her PhD scholarship. Y. G. thanks the European Union's Horizon research and innovation programme under the Marie Skłodowska-Curie grant agreement no. 10115148 (LEK-PV). The authors from UPC belong to the Micro and Nanotechnologies for Solar Energy Group (MNTSolar), a Consolidated Research Group of the "Generalitat de Catalunya" (2021 SGR 01286). This work is also part of the Maria de Maeztu Units of Excellence Programme CEX2023-001300-M,funded by MICIU/AEI/10.13039/501100011033. E. S. is grateful to ICREA Academia program. This work was also supported by the "MUSA—Multilayered Urban Sustainability Action" project, funded by the European Union, *via* NextGenerationEU, under the National Recovery and Resilience Plan (NRRP) Mission 4 Component 2 Investment Line 1.5: Strengthening of research structures and creation of R&D "innovation ecosystems", and set up of "territorial leaders in R&D". The article is based upon work from the COST Action Research and International Networking project "Emerging Inorganic Chalcogenides for PVs (RENEW-PV)," CA21148, supported by COST (European Cooperation in Science and Technology).

Notes and references

1 J. Li, K. Sun, X. Yuan, J. Huang, M. A. Green and X. Hao, *npj Flexible Electronicsnpj Flexible Electron.*, 2023, **7**, 16.
2 H. Deng, Q. Sun, Z. Yang, W. Li, Q. Yan, C. Zhang, Q. Zheng, X. Wang, Y. Lai and S. Cheng, *Nat. Commun.*, 2021, **12**, 3107.
3 X. Li, P. Li, Z. Wu, D. Luo, H.-Y. Yu and Z.-H. Lu, *Mater. Rep.: Energy*, 2021, **1**, 100001.
4 J.-H. Min, W.-L. Jeong, K. Kim, J.-S. Lee, K.-P. Kim, J. Kim, M. G. Gang, C. W. Hong, J. H. Kim and D.-S. Lee, *ACS Appl. Mater. Interfaces*, 2020, **12**, 8189–8197.
5 W. Xie, Q. Yan, Q. Sun, Y. Li, C. Zhang, H. Deng and S. Cheng, *Sol. RRL*, 2023, **7**, 2201036.
6 M. Rehan, A. Cho, I. Jeong, K. Kim, A. Ullah, J.-S. Cho, J. H. Park, Y. Jo, S. J. Hong, S. K. Ahn, S. Ahn, J. H. Yun, J. Gwak and D. Shin, *Energy Environ. Mater.*, 2024, **7**, e12604.
7 S. K. Hwang, S. J. Park, J. H. Park, J. H. Yoon, J. Yu Cho, D. K. Cho, J. Heo, G. Y. Kim and J. Y. Kim, *Small*, 2024, **20**, 2307175.
8 A. Jimenez-Arguijo, A. G. Medaille, A. Navarro-Güell, M. Jimenez-Guerra, K. J. Tiwari, M. Placidi, M. S. Mkehlane, E. Iwuoha, A. Perez-Rodriguez, E. Saucedo, S. Giraldo and Z. Jehl Li-Kao, *Sol. Energy Mater. Sol. Cells*, 2023, **251**, 112109.

9 E. Jo, M. G. Gang, H. Shim, M. P. Suryawanshi, U. V. Ghorpade and J. H. Kim, *ACS Appl. Mater. Interfaces*, 2019, **11**, 23118–23124.
10 M. A. Olgar, S. Erkan and R. Zan, *J. Alloys Compd.*, 2025, **1011**, 178346.
11 Y. Gong, Y. Zhang, E. Jedlicka, R. Giridharagopal, J. A. Clark, W. Yan, C. Niu, R. Qiu, J. Jiang, S. Yu, S. Wu, H. W. Hillhouse, D. S. Ginger, W. Huang and H. Xin, *Sci. China Mater.*, 2021, **64**, 52–60.
12 C. Gobbo, V. Di Palma, V. Trifiletti, C. Malerba, M. Valentini, I. Matacena, S. Daliento, S. Binetti, M. Acciarri and G. Tseberlidis, *Energies*, 2023, **16**, 4137.
13 G. Tseberlidis, V. Di Palma, V. Trifiletti, L. Frioni, M. Valentini, C. Malerba, A. Mittiga, M. Acciarri and S. O. Binetti, *ACS Mater. Lett.*, 2023, **5**, 219–224.
14 G. Tseberlidis, C. Gobbo, V. Trifiletti, V. Di Palma and S. Binetti, *Sustainable Mater. Technol.*, 2024, **41**, e01003.
15 M. A. Green, E. D. Dunlop, M. Yoshita, N. Kopidakis, K. Bothe, G. Siefer, X. Hao and J. Y. Jiang, *Prog. Photovolt.: Res. Appl.*, 2025, **33**, 795–810.
16 X. Xu, J. Zhou, K. Yin, J. Wang, L. Lou, D. Li, J. Shi, H. Wu, Y. Luo and Q. Meng, *Adv. Energy Mater.*, 2023, **13**(38), 2301701.
17 H. K. Park, Y. Cho, J. Kim, S. Kim, S. Kim, J. Kim, K.-J. Yang, D.-H. Kim, J.-K. Kang and W. Jo, *npj Flexible Electron.*, 2022, **6**, 91.
18 H. K. Park, Y. Cho, J. Kim, G. Y. Kim, W.-L. Jeong, K.-P. Kim, D.-S. Lee and W. Jo, *Sol. Energy Mater. Sol. Cells*, 2021, **230**, 111243.
19 Y. Gong, R. Qiu, C. Niu, J. Fu, E. Jedlicka, R. Giridharagopal, Q. Zhu, Y. Zhou, W. Yan, S. Yu, J. Jiang, S. Wu, D. S. Ginger, W. Huang and H. Xin, *Adv. Funct. Mater.*, 2021, **31**, 2101927.
20 Y. Gong, A. Jimenez-Arguijo, A. G. Medaille, S. Moser, A. Basak, R. Scaffidi, R. Carron, D. Flandre, B. Vermang, S. Giraldo, H. Xin, A. Perez-Rodriguez and E. Saucedo, *Adv. Funct. Mater.*, 2024, **34**, 2404669.
21 J. J. Scragg, J. T. Wätjen, M. Edoff, T. Ericson, T. Kubart and C. Platzer-Björkman, *J. Am. Chem. Soc.*, 2012, **134**, 19330–19333.
22 J. Lin, X. Wu, J. Xu and Y. Yang, *Opt. Mater.*, 2022, **124**, 111996.
23 V. Karade, A. Lokhande, P. Babar, M. G. Gang, M. Suryawanshi, P. Patil and J. H. Kim, *Sol. Energy Mater. Sol. Cells*, 2019, **200**, 109911.
24 C. Platzer-Björkman, N. Barreau, M. Bär, L. Choubrac, L. Grenet, J. Heo, T. Kubart, A. Mittiga, Y. Sanchez, J. Scragg, S. Sinha and M. Valentini, *JPhys Energy*, 2019, **1**, 044005.
25 J. Fu, A. Zhang, D. Kou, Z. Xiao, W. Zhou, Z. Zhou, S. Yuan, Y. Qi, Z. Zheng and S. Wu, *Chem. Eng. J.*, 2023, **457**, 141348.
26 S. López-Marino, M. Placidi, A. Pérez-Tomás, J. Llobet, V. Izquierdo-Roca, X. Fontané, A. Fairbrother, M. Espíndola-Rodríguez, D. Sylla, A. Pérez-Rodríguez and E. Saucedo, *J. Mater. Chem. A*, 2013, **1**, 8338.
27 T. Schnabel and E. Ahlswede, *Sol. Energy Mater. Sol. Cells*, 2017, **159**, 290–295.
28 Y. Li, H. Wei, C. Cui, X. Wang, Z. Shao, S. Pang and G. Cui, *J. Mater. Chem. A*, 2023, **11**, 4836–4849.
29 S.-Z. Xu, Y.-P. Song, B. Yao, M.-G. Li, Z.-H. Ding, R. Deng, H.-N. Liang, X.-B. Du and Y.-F. Li, *ACS Appl. Mater. Interfaces*, 2024, **16**, 11026–11034.
30 L. Liu, T.-K. Lau, Z. Zhi, L. Huang, S. Wang and X. Xiao, *Sol. RRL*, 2018, **2**, 1800243.
31 Z. Su, W. Xie, Q. Sun, Y. Li, Z. Zhong, W. Wang, C. Zhang, H. Deng and S. Cheng, *ACS Mater. Lett.*, 2025, **7**, 1329–1335.
32 Y. Li, C. Cui, H. Wei, Z. Shao, Z. Wu, S. Zhang, X. Wang, S. Pang and G. Cui, *Adv. Mater.*, 2024, **36**, 2400138.
33 A. Zhang, Z. Zhou, W. Zhou, D. Kou, Y. Meng, Y. Qi, S. Yuan and S. Wu, *Sol. RRL*, 2019, **3**, 1900131.
34 P. D. Antunez, D. M. Bishop, Y. S. Lee, T. Gokmen, O. Gunawan, T. S. Gershon, T. K. Todorov, S. Singh and R. Haight, *Adv. Energy Mater.*, 2017, **7**, 1602585.
35 A. Wang, M. He, M. A. Green, K. Sun and X. Hao, *Adv. Energy Mater.*, 2023, **13**, 2203046.
36 K. Yang, S. Kim, S. Kim, D. Son, J. Lee, Y. Kim, S. Sung, D. Kim, T. Enkhbat, J. Kim, J. Kim, W. Jo and J. Kang, *Adv. Funct. Mater.*, 2021, **31**, 2102238.
37 C. Zhang, W. Xu, Q. Sun, Z. Zhong, W. Xie, Y. Li, Z. Su, Y. Zhang, H. Deng, W. Wang and S. Cheng, *Appl. Surf. Sci.*, 2025, **692**, 162738.
38 H. Xu, R. Meng, X. Xu, L. Wu, Y. Sun, Y. Liu, Z. Wang, N. Wang, M. Li and Y. Zhang, *Small Methods*, 2025, **9**, 2401084.
39 Y. Zhang, Q. Sun, W. Xie, Y. Li, Z. Su, W. Xu, W. Wang, H. Deng and S. Cheng, *J. Energy Chem.*, 2025, **105**, 806–813.
40 Y. Gong, Y. Zhang, Q. Zhu, Y. Zhou, R. Qiu, C. Niu, W. Yan, W. Huang and H. Xin, *Energy Environ. Sci.*, 2021, **14**, 2369–2380.
41 Y. Gong, Q. Zhu, B. Li, S. Wang, B. Duan, L. Lou, C. Xiang, E. Jedlicka, R. Giridharagopal, Y. Zhou, Q. Dai, W. Yan, S. Chen, Q. Meng and H. Xin, *Nat. Energy*, 2022, **7**, 966–977.
42 M. He, X. Zhang, J. Huang, J. Li, C. Yan, J. Kim, Y.-S. Chen, L. Yang, J. M. Cairney, Y. Zhang, S. Chen, J. Kim, M. A. Green and X. Hao, *Adv. Energy Mater.*, 2021, **11**, 2003783.
43 H. Xin, S. M. Vorpahl, A. D. Collord, I. L. Braly, A. R. Uhl, B. W. Krueger, D. S. Ginger and H. W. Hillhouse, *Phys. Chem. Chem. Phys.*, 2015, **17**, 23859–23866.
44 Y. Yang, L. Huang and D. Pan, *ACS Appl. Mater. Interfaces*, 2017, **9**, 23878–23883.
45 M. Dimitrievska, F. Oliva, M. Guc, S. Giraldo, E. Saucedo, A. Pérez-Rodríguez and V. Izquierdo-Roca, *J. Mater. Chem. A*, 2019, **7**, 13293–13304.
46 S. Gao, Y. Zhang, J. Ao, S. Lin, Z. Zhang, X. Li, D. Wang, Z. Zhou, G. Sun, F. Liu and Y. Sun, *Sol. Energy Mater. Sol. Cells*, 2018, **176**, 302–309.
47 S. Lopez-Marino, M. Espíndola-Rodríguez, Y. Sánchez, X. Alcobé, F. Oliva, H. Xie, M. Neuschitzer, S. Giraldo, M. Placidi, R. Caballero, V. Izquierdo-Roca, A. Pérez-Rodríguez and E. Saucedo, *Nano Energy*, 2016, **26**, 708–721.
48 X. S. Wu and J. X. Xu, *Chalcogenide Lett.*, 2022, **19**, 599–609.
49 S. Ge, H. Xu, S. N. Khan, W. Yang, R. Hong, Y. Mai, E. Gu, X. Lin and G. Yang, *Sol. RRL*, 2021, **5**, 2100598.

50 F. Liu, J. Huang, K. Sun, C. Yan, Y. Shen, J. Park, A. Pu, F. Zhou, X. Liu, J. A. Stride, M. A. Green and X. Hao, *NPG Asia Mater.*, 2017, **9**, e401.
51 X. Li, C. Ma, N. Liu, C. Xiang, S. Wei, W. Yan, W. Huang and H. Xin, *Adv. Funct. Mater.*, 2024, **34**, 2310124.
52 S. Ranjbar, G. Brammertz, B. Vermang, A. Hadipour, S. Cong, K. Suganuma, T. Schnabel, M. Meuris, A. F. da Cunha and J. Poortmans, *Phys. Status Solidi A*, 2017, **214**, 1600534.
53 A. Cabas-Vidani, L. Choubrac, J. A. Márquez, T. Unold, M. Maiberg, R. Scheer, H. Li, K. Leifer, R. Pauer, E. Gilshtein, A. N. Tiwari and Y. E. Romanyuk, *ACS Appl. Mater. Interfaces*, 2021, **13**, 19487–19496.
54 C. Zhang, Z. Yang, H. Deng, Q. Yan, W. Xie, Q. Sun, X. Sheng and S. Cheng, *J. Phys. Chem. C*, 2021, **125**, 16746–16752.
55 A. T. Neal, R. Pachter and S. Mou, *Appl. Phys. Lett.*, 2017, **110**, 193103.
56 X. Sun, L. Yu, F. Yang, X. Dong, J. Chen, X. Zhang, Y. Zhao and Y. Li, *Sol. Energy Mater. Sol. Cells*, 2022, **248**, 112034.
57 K. Ahn, S.-Y. Kim, S. Kim, D.-H. Son, S.-H. Kim, S. Kim, J. Kim, S.-J. Sung, D.-H. Kim and J.-K. Kang, *J. Mater. Chem. A*, 2019, **7**, 24891–24899.
58 Q. Zhao, H. Shen, Y. Xu, K. Gao, D. Chen and Y. Li, *ACS Appl. Energy Mater.*, 2022, **5**, 3668–3676.
59 I. Becerril-Romero, L. Acebo, F. Oliva, V. Izquierdo-Roca, S. López-Marino, M. Espíndola-Rodríguez, M. Neuschitzer, Y. Sánchez, M. Placidi, A. Pérez-Rodríguez, E. Saucedo and P. Pistor, *Prog. Photovolt.: Res. Appl.*, 2018, **26**, 55–68.